Do Low-Cost Seismographs Perform Well Enough for Your Network? An Overview of Laboratory Tests and Field Observations of the OSOP Raspberry Shake 4D

by Robert E. Anthony, Adam T. Ringler, David C. Wilson, and Emily Wolin

ABSTRACT

Seismologists have recently begun using low-cost nodal sensors in dense deployments to sample the seismic wavefield at unprecedented spatial resolution. Earthquake early warning systems and other monitoring networks (e.g., wastewater injection) would also benefit from network densification; however, current nodal sensors lack power systems or the real-time data transmission required for these applications. A candidate sensor for these networks may instead be a low-cost, all-in-one package such as the OSOP Raspberry Shake 4D (RS-4D). The RS-4D includes a vertical-component geophone, three-component accelerometer, digitizer, and near-real-time miniSEED data transmission and costs only a few hundred dollars per unit. Here, we step through instrument testing of three RS-4Ds at the Albuquerque Seismological Laboratory (ASL). We find that the geophones have sensitivities constrained to within 4% of nominal, but that they have relatively high self-noise levels compared with the broadband sensors typically used in seismic networks. To demonstrate the impact this would have on characterizing nearby events, we estimate local magnitudes of earthquakes in Oklahoma using Trillium Compact broadband sensor data from U.S. Geological Survey aftershock deployments as well as 23 Raspberry Shakes operated by hobbyists and private owners within the state. We find that for M_L 2.0–4.0 earthquakes at distances of 20–100 km from seismic stations, the Raspberry Shakes require events of magnitude ~0.3 larger than the broadband sensors to reliably estimate M_L at a given distance from the epicenter. We conclude that RS-4Ds are suitable for densifying backbone networks designed for studies of local and regional events.

INTRODUCTION

The choice of which seismic instrumentation to purchase for a seismic network or field study is filled with trade-offs. Size, ease of deployment, power consumption, data format and storage, cost, and performance of the sensor must all be taken into account. Of these, performance of the system in terms of noise, dynamic range, and ability to recover true ground motion across a broad range of frequencies may be the most difficult for researchers to intuit and assess. However, the best-performing sensors are not needed for all applications, which is advantageous because sensor performance is often a direct trade-off with sensor cost. Thus, to maximize use of available funds while still accomplishing the goal of recording the seismic signal of interest with acceptable fidelity, it is necessary for network designers and researchers to understand how sensor performance is measured and the meanings of the various metrics used to quantify this performance. Additionally, data users must understand any limitations in the fidelity of seismic waveforms that arise through the performance of different sensors.

Recently, seismologists have begun rapidly exploiting relatively low-cost, easily deployable geophone packages, referred to as nodes, in temporary seismic deployments. The low cost of nodes coupled with the ability to install the instruments quickly has led to large numbers of sensors (> 100) being deployed in spatially dense (< 200 m station spacing) networks (e.g., Schmandt and Clayton, 2013; Ben-Zion *et al.*, 2015; Sweet *et al.*, 2018). In turn, this has enabled high-resolution imaging of the shallow subsurface (e.g., Lin *et al.*, 2013), reduced detection thresholds of local seismicity (e.g., Hansen and Schmandt, 2015), and improved characterization of naturally occurring and anthropogenic high-frequency (> 1 Hz) seismic noise sources (e.g., Riahi and Gerstoft, 2015; Schmandt *et al.*, 2017).

Low-cost sensors may have additional utility in increasing the spatial density of earthquake monitoring networks, including earthquake early warning systems (EEWSs), monitoring of wastewater injection sites, and aftershock deployments. Besides enabling the detection and location of smaller events, this additional instrumentation has the potential to improve EEWSs by reducing the spatial area near the earthquake epicenters that would receive no warning before extreme ground motion (Kuyuk and Allen, 2013). However, despite having acceptable high-frequency sensor performance to capture these local events (Ringler *et al.*, 2018), the current nodal sensors used by the seismological community are likely not suitable for

doi: 10.1785/0220180251

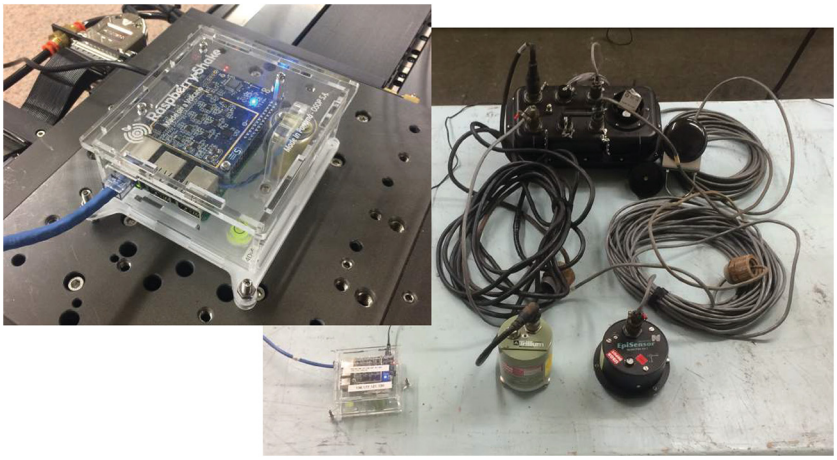

▲ **Figure 1.** A Raspberry Shake 4D (RS-4D) (upper-left inset) compared to the equipment used in a typical U.S. Geological Survey (USGS) aftershock deployment. Both systems incorporate a seismometer, three-component accelerometer, 24-bit digitizer, and timing information. However, the RS-4D is more than an order of magnitude less expensive.

long-term monitoring applications because of their relatively short battery lives (~1 month), the inability to transmit data in real time, and the clip level being lower than required for near-source recordings. Instead, the recently developed OSOP Raspberry Shake (Fig. 1) and other low-cost microelectromechanical systems (MEMSs) accelerometer packages have been proposed as candidate low-cost (< 1000 U.S.) sensor and digitizer packages for densifying earthquake monitoring networks because they use an external power source and are designed to transmit near-real-time data (Evans *et al.*, 2014).

Here, we evaluate the performance of three Raspberry Shake 4D (RS-4D; v. 5) seismographs through a series of laboratory tests at Albuquerque Seismological Laboratory (ASL). For comparative purposes, these metrics are referenced to a typical U.S. Geological Survey (USGS) aftershock station, which we note is more than an order of magnitude more expensive. Although our findings are recapped in the Summary of Instrument Performance section at the end of the article, here we describe how and why these tests are performed. We additionally estimate local earthquake magnitudes in Oklahoma with both USGS aftershock deployment stations and public data from personal Raspberry Shakes deployed in the state. Our goal is to provide seismologists with the information necessary to determine if the RS-4D and similar sensors are suitable for use in their networks and to explain how sensors are evaluated in laboratory tests to yield information about our ability to resolve ground motion.

USGS AFTERSHOCK DEPLOYMENT VERSUS RS-4D

The instrumentation currently used in USGS aftershock deployments is shown in Figure 1 and consists of a three-component broadband seismometer (Nanometrics Trillium Compact 120-s high-pass corner), a three-component accelerometer (Kinemetrics EpiSensor 4g) for recording strong ground motion, a 24-bit digitizer (RefTek RT-130 digitizer), and a Global Positioning System (GPS) antenna for timing. Power is typically supplied by lead-acid batteries connected to a solar panel (not pictured), and real-time data transmission is often achieved through a cell modem or wireless router connecting to the landowner's private network. We note that on RT-130s, data may also be stored locally on flash cards. The total cost for a USGS aftershock station is a couple tens of thousands of U.S. dollars.

In contrast, the sensors in the RS-4D include a vertical-component 4.5-Hz geophone with the corner frequency electronically extended to 0.5 Hz (e.g., Romeo, 2012) and a three-component MEMS accelerometer. The internal digitizer is 24 bit, and the recorded 100-Hz data may be stored either locally on a flash drive and external Universal Serial Bus (USB) memory stick or transmitted in near-real time (4-Hz packet transfer rate) through a local network in miniSEED (Seismic Exchange for Earthquake Data) format (Ahern *et al.*, 2009). The RS-4D also uses this network connection to provide time stamping of the data using network timing protocol (NTP), although an optional GPS antenna may be purchased separately to provide a pulse per second timing signal (see Data and Resources for link to Raspberry Shake technical specifications). Out of the box, power is supplied by a transformer that converts alternating current (AC) power from a typical wall outlet to 5-V, 2.5-A (12-W) direct current power channeled through a micro USB port. Although it would be possible to power and provide continuous data from the RS-4D in remote environments, the sensor was designed to be installed within infrastructure with reliable network connectivity and AC power. The cost of an RS-4D ranges from a few hundred to approximately $1000 U.S. depending on whether a GPS antenna and all-weather enclosures are purchased for the unit.

LABORATORY TESTS AND RESULTS

Self-Noise

All seismometers and digitizers generate internal noise through both their electronics and thermally induced motion of the masses (e.g., Aki and Richards, 2002). This noise is frequency dependent, often increasing drastically at lower frequencies (e.g., Sleeman *et al.*, 2006), and defines the lower limit of ground motions that can be detected by the instrument. Signals falling well below (> ~5 dB) the self-noise level of an instrument will not be recorded, and signals with similar amplitudes as the self-noise level will be recorded with poor fidelity and become difficult to decipher. Thus, it is imperative that seismologists choose instrumentation that has self-noise levels well below the signal of interest. Additionally, reasonable care

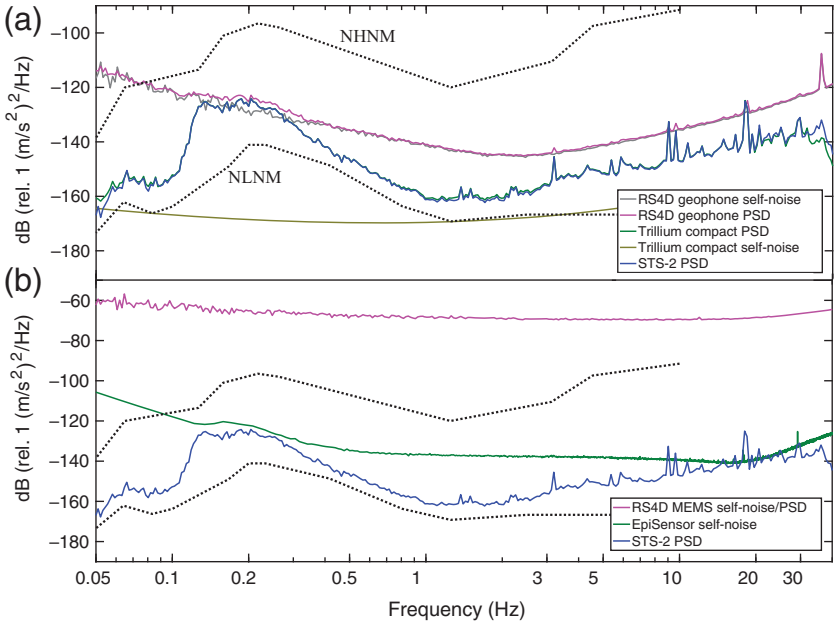

▲ **Figure 2.** Self-noise estimates of the (a) RS-4D vertical-component geophone and (b) accelerometer using a six-hour time window and the methodology of Sleeman *et al.* (2006). For comparative purposes, we included the power spectral density (PSD) estimates over the same six-hour window for a variety of collocated seismic instruments, the median self-noise models for a Nanometrics Trillium Compact (Ringler and Hutt, 2010), and a Kinemetrics EpiSensor (Ringler *et al.*, 2015), as well as the new high- and low-noise models (NHNMs/NLNMs; Peterson, 1993).

should be taken to isolate the sensors from seismic and nonseismic noise sources such as wind (e.g., Hutt *et al.*, 2017), cultural noise (e.g., Anthony *et al.*, 2015), thermal variations (e.g., Doody *et al.*, 2017), and atmospheric pressure variations (e.g., Wolin *et al.*, 2015).

To estimate the self-noise of the RS-4D, we collocated three of these sensors in a surface vault at ASL and used three-channel correlation analysis (Sleeman *et al.*, 2006) over a six-hour time period free from transient signals (e.g., people entering the vault, earthquakes). This methodology assumes that true ground motion will appear as a coherent signal on the three RS-4Ds and attributes incoherent signals as self-noise of the instruments. For comparative purposes, we provide estimates of ambient ground motion attained by collocating a broadband Streckeisen STS-2 attached to a Quanterra Q330 digitizer recording at 200 Hz with the RS-4Ds. We note that a STS-2 recording on a Q330 has significantly lower self-noise levels than background ground motion at ASL over the frequency band considered here (Ringler and Hutt, 2010). Additionally, a Trillium Compact was collocated with the sensors, and we provide the median self-noise estimates of a Trillium Compact from Ringler and Hutt (2010). The power spectral densities (PSDs) and self-noise estimates presented here are given in decibels (relative to 1 $(m^2/s^4)/Hz$) and have been smoothed across 1/64th octave windows using the algorithm from the Incorporated Research Institutions for Seismology noise tool kit (Incorporated Research Institutions for Seismology Data Management Center [IRIS-DMC], 2014).

With the exception of the ~0.1- to 0.2-Hz secondary microseism peak (e.g., Peterson, 1993) and narrowband sources of high-frequency energy at 9 and 18 Hz, ambient ground motion in the surface vault falls below the self-noise level of the RS-4D geophone and is not recorded (Fig. 2a). Furthermore, because the secondary microseism peak during this time window only exceeds the self-noise level of the geophone by ~3 dB, the self-noise of the sensor contributes to the PSD estimate in this band. This results in overestimation of secondary microseism amplitudes relative to the reference STS-2. In contrast, the Trillium Compact records nearly identical ground motions as the STS-2 from ~0.07 to 30 Hz because of the much lower self-noise levels of this sensor.

A peak in both the self-noise and the PSD of the RS-4Ds at 36 Hz is the result of internal noise from the digitizer that is referred to as an "idle tone" (Reiss, 2008; A. Rodriguez and B. Christensen, written comm., 2017). We note that earlier versions of the Raspberry Shake tested at ASL exhibited lower frequency idle tones between 0.2 and 5 Hz that were unique to each unit. These lower frequency idle tones should only be present on v. 4 and 5 of the Raspberry Shake 1D (RS-1D), a sensor similar to the RS-4D but without the MEMS accelerometers. Sensors produced after mid-2018 should have the idle tone issue resolved all together (B. Christensen, written comm., 2018).

Idle tones are not present on the MEMS accelerometer because the high self-noise levels of these sensors exceeds the idle tone noise by > 40 dB (Fig. 2b). Over the range of 1–20 Hz, self-noise levels of the RS-4D accelerometer exceed those of the EpiSensor by > 65 dB, and no ambient ground motion was recorded by these sensors while they were deployed in our surface vault. The accelerometers failed to record a local (< 10 km) M_D 1.7 event, and we roughly estimate that local events below M 2.5 and regional (~100 km) events below M 5.0 will not be recorded on the accelerometer channels (e.g., Clinton and Heaton, 2002).

Dynamic Range and Clip Levels

While the self-noise levels of a sensor constrain the lowest possible ground motion a sensor can record, the highest possible signal is bound by the clip level of the sensor. Together, these two parameters define the dynamic range of the sensor. The dynamic range (D_R) is typically reported in decibels at a given frequency (f) and is calculated as:

$$D_R(f) = 20 \log_{10}\left(\frac{A_C(f)}{A_N(f)}\right),$$

in which A_C is the clip level amplitude and A_N is the amplitude of the noise floor at the frequency of interest. Because the

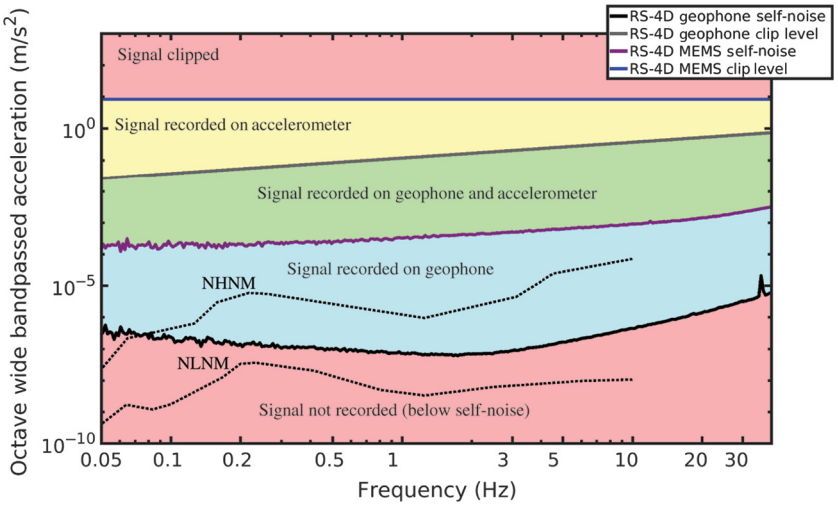

▲ **Figure 3.** Self-noise and clip levels for the RS-4D geophone and vertical accelerometer plotted in one-octave acceleration amplitudes as a function of frequency (after Steim, 1986). For reference, the Peterson (1993) NHNMs/NLNMs are additionally plotted. At 1 Hz, the geophone has 130 dB of dynamic range, and the accelerometer has 94 dB.

self-noise levels are estimated as an acceleration PSD and clip levels are an amplitude measurement, all quantities are converted to amplitudes. This is accomplished by integrating the PSD estimates over 1-octave bands and enables direct comparison with the clip levels (Fig. 3, Steim, 1986; Clinton and Heaton, 2002).

We determine the clip levels of the RS-4D by bolting it to an aluminum plate along with a 4-g Kinemetrics EpiSensor and subjecting both instruments to strong motion. The clip levels were then determined by observing the maximum velocity or acceleration that the RS-4D could output. We found that the geophone could reliably record velocities up to 22 mm/s and that the accelerometers could record vertical accelerations up to 1 *g* and horizontal accelerations up to 2 *g*. The discrepancy in clip levels for the accelerometer components arises because the RS-4D installed in a normal configuration always registers 1 *g* of positive acceleration due to gravity. Thus, the 2-*g* accelerometer can only sustain another 1 *g* of positive acceleration before clipping occurs. Assuming these minimum clip levels, we arrived at a dynamic range at 1 Hz of 130 dB (~21.5 bits of resolution) for the geophone, 94 dB (~15.6 bits of resolution) for the vertical accelerometer, and 100 dB (~16.6 bits of resolution) for the horizontal accelerometers.

For comparison, a Trillium Compact seismometer has a slightly higher nominal clip level of 26 mm/s and a much larger dynamic range of ~152 dB at 1 Hz. This larger dynamic range is a direct result of the lower self-noise of the sensor. The EpiSensor accelerometer typically used in USGS aftershock deployments has a user-selectable clip level of up to 4 *g* and a specified dynamic range of 155 dB. We note that the Advanced National Seismic System (ANSS) requires accelerometers used in both regional and urban monitoring stations to have a minimum clip level of 3.5 *g* (Advanced National Seismic System [ANSS] Working Group, 2008).

INSTRUMENT RESPONSE

Obtaining measurements of ground motion in physical units (i.e., displacement, velocity, or acceleration) is essential for many seismological applications. Because most modern seismic equipment records signals in units of digital counts, seismologists must be able to correctly deconvolve the response of the instrument to attain estimates of true ground motion. Any errors in the instrument response will be directly propagated to ground-motion estimates. General practice within the seismological community is to assume that the response of any individual sensor is accurately described by the manufacturer-specified nominal response (e.g., Templeton, 2017). Here, we derive the response of the RS-4D from first principles with the goal of observing both how accurately the nominal response is characterized as well as how much the response varies between individual sensors.

Typically, the response of seismic recording systems is broken down into the broad categories of (1) a frequency-dependent amplitude and phase response of the sensor as ground motion is converted into an analog voltage and (2) a scalar conversion factor as this voltage is converted into counts by the digitizer. The digitizer gain can usually be determined with extreme accuracy (< 0.2%, Anthony *et al.*, 2017) by inputting a precisely known voltage into the digitizer and recording the output. However, this is not easily accomplished on the RS-4D because the sensors and digitizer are directly connected from the factory as a single, integrated unit. Thus, we incorporate the digitizer gain into the frequency-dependent amplitude response and report the sensitivity in units of counts per m/s for the geophone and m/s^2 for the accelerometer.

Because accelerometers generally have a flat response out to 0 Hz (e.g., Evans *et al.*, 2014) and the nominal high-frequency corner is close to the Nyquist frequency of the Raspberry Shake (50 Hz), we do not estimate the frequency-dependent response of the MEMS accelerometers. To attain the sensitivities of the MEMS accelerometers, we attached each sensor to a box with precisely squared faces and flipped it over. This inverted each axis of the accelerometer such that each component observed an acceleration change of 2 *g* (e.g., Evans *et al.*, 2014). Because the value of *g* (9.79188087 m/s^2) has been precisely measured at ASL by an absolute gravimeter, this method is capable of performing absolute calibrations of accelerometers to < 0.1% accuracy (Anthony *et al.*, 2017). We tested all three RS-4Ds and observed 1.5% variability in the sensitivity of the nine components (Table 1). We found that our determined sensitivities are systematically ~4.3% higher than the nominal sensitivity reported by OSOP.

Unlike accelerometers, geophones and broadband seismometers are not capable of recording variations in acceleration of 2 *g*. Instead, the sensitivity of these instruments is often determined by

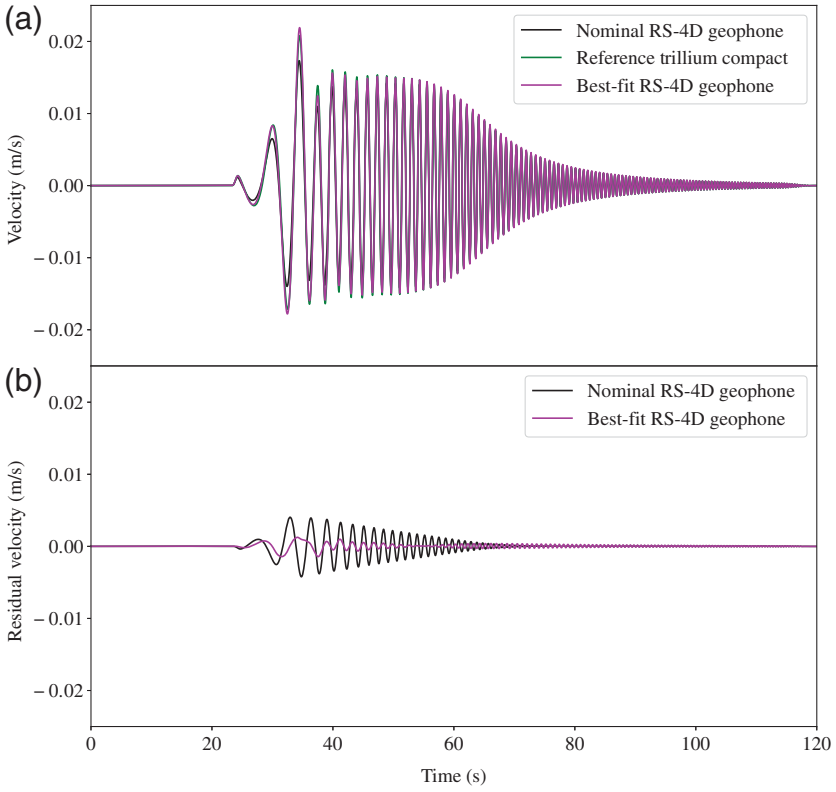

▲ **Figure 4.** (a) An example of the 0.1- to 10-Hz shake table swept sinusoid test used to determine the sensitivity, damping, and free period of the RS-4D geophone. The waveforms here have been filtered between 0.3 and 2 Hz to isolate the corner frequency of the RS-4D geophone (~0.5 Hz). (b) The response of the RS-4D is inverted for by minimizing its residual waveforms with a Nanometrics Trillium Compact reference sensor, with a known response.

collocating them with a reference sensor and subjecting both sensors to coherent ground motion (e.g., Pavlis and Vernon, 1994). For most broadband sensors, this can be readily accomplished in a vault using secondary microseisms (e.g., Ringler *et al.*, 2017). However, the high self-noise levels of the RS-4D geophones obscure true microseism amplitudes (Fig. 2a). To generate coherent signals well above the self-noise levels of the RS-4D geophone, we attach the sensor next to a Trillium Compact on a vertical shake table and drive the table with a constant velocity (0.015 m/s 0-to-peak) swept sine wave (0.1–10 Hz, Fig. 4). The amplitude and phase response of the geophone can be modeled as a damped harmonic oscillator, which can be described by its free period, damping ratio, and sensitivity (i.e., gain or the conversion factor from digital counts to m/s in the flat band of the response; Romeo, 2012). We use a swept sine input signal encompassing the corner frequency of the geophone so that we can simultaneously invert for these three parameters (Ringler *et al.*, 2018).

To process the shake table data, we select a 2-min window of data beginning 20 s before the start of the shake test. We then remove the nominal response of the reference Trillium Compact (Templeton, 2017) using the nominal parameters for the ObsPy deconvolution routine (Krischer *et al.*, 2015), apply a 5% cosine taper to the signal, and bandpass filter from 0.3 to 2 Hz. The response of the reference Trillium Compact has been previously calibrated using an absolute gravity method and was found to match nominal to $< 1\%$ (Anthony *et al.*, 2017). Finally, we estimate the best-fit parameters using the downhill simplex algorithm (Nelder and Mead, 1965) to minimize the residual between the waveforms of the Trillium Compact and the Raspberry Shake geophone. This method is similar to CALEX used in Wielandt and Zumberge (2013). Because geophones are often critically damped, we used 0.707 as an ini-

Table 1
Instrument Response of Three Raspberry Shake Sensors as Determined through Testing at Albuquerque Seismological Laboratory (ASL)

Raspberry Shake 4D Station Name	Accelerometer Sensitivity (Counts/(m/s^2))	Geophone Sensitivity (Counts/(m/s))	Geophone Free-Period (Hz)	Geophone Damping
Nominal	386,825	335,815,000	0.57	0.707
RB7A0	N: 400,600 E: 401,900 Z: 401,800	331,383,000	0.55	0.792
R5D49	N: 405,700 E: 402,600 Z: 406,500	348,314,000	0.59	0.848
R141E	N: 401,400 E: 403,300 Z: 406,300	329,623,000	0.57	0.809

Accelerometer sensitivities are given for the north (N), east (E), and vertical (Z) components.

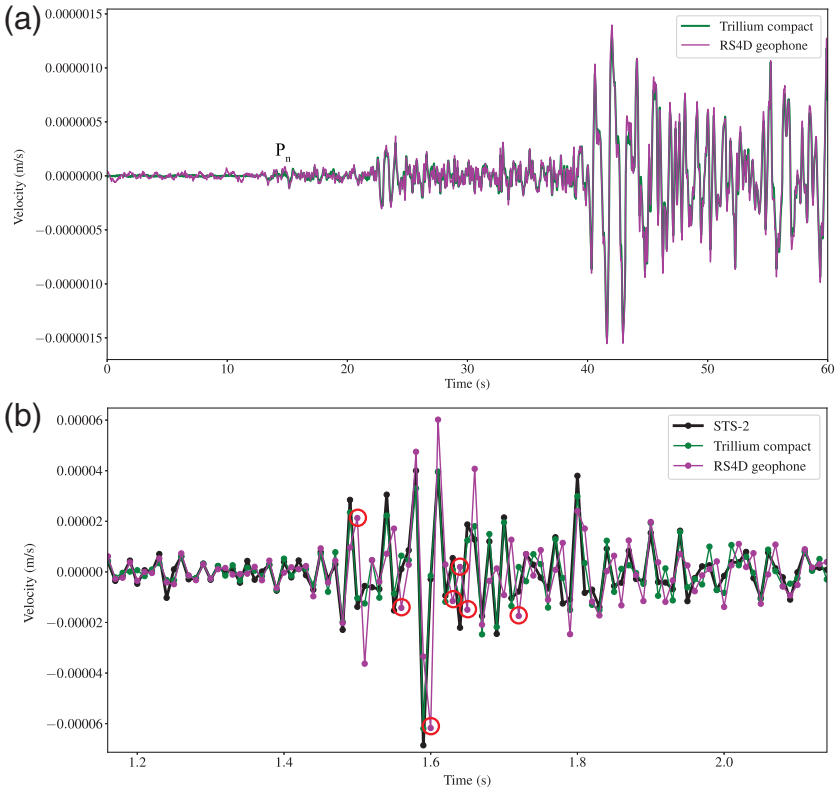

▲ **Figure 5.** (a) The *P*-wave arrivals of a regional (7.4°) M_w 4.6 event in Oklahoma recorded at Albuquerque Seismological Laboratory (ASL) on a collocated OSOP RS-4D and Nanometrics Trillium Compact. The first phase arrival (P_n) is labeled for reference. (b) The *S*-wave arrival of an M_D 1.7 local event recorded on three collocated seismometers in the surface vault of ASL. The Streckeisen STS-2 and Trillium Compact were recording on a Q330 digitizer with timing accurate to ≪ 1 ms (Kromer, 2006). Red circles indicate samples from the RS-4D that appear to have a one sample (10 ms) lag compared to the other instruments.

tial guess for the damping parameter. The initial guesses of 0.5 Hz for the free period and 335,815,000 counts/(m/s) for the sensitivity were based off the nominal response for the RS-4D provided by OSOP.

The results of the shake table test are shown in Table 1. Overall, we found that the sensitivity of three RS-4D geophones varied by 5.7% and were within 4% of the OSOP-specified nominal sensitivity. For comparison, two Trillium Compacts calibrated in a similar fashion had a variability of 1.0% and deviated from the manufacturer-specified nominal sensitivity by no more than 0.8% (Anthony *et al.*, 2017). All of the RS-4D geophones were found to be slightly overdamped with a 7% range in damping constants. Finally, the mean free period of the RS-4D geophone was found to be 0.57 Hz with a range of 7%.

For most applications, the manufacturer-specified nominal response for the RS-4D will likely be sufficient. Figure 5a shows several *P*-wave phase arrivals from a regional (7.4°) M_w 4.6 earthquake in Oklahoma recorded on both the reference Trillium Compact and an RS-4D at ASL using the RS-4D nominal response. The waveforms from both sensors have been bandpass filtered between 0.5 and 10 Hz to remove longer period signals that are recorded on the Trillium Compact but fall below the self-noise levels of the RS-4D. Visually, the waveforms have excellent coherence with slight deviations occurring due to timing errors and noise on the RS-4D as discussed in the following sections.

TIMING ACCURACY

Measuring accurate arrival times of seismic waveforms is of crucial importance in many seismological studies, such as locating earthquakes and body-wave tomography. The internal NTP server on the RS-4D maintains accurate timing by continually correcting for the timing offsets between itself and a reference clock (e.g., see Data and Resources). Internal logs of these timing offsets examined on seismic stations within the South Carolina Earth Physics Project network suggested that NTP timing errors are generally below 20 ms and are roughly symmetrically distributed about 0 ms (Frassetto *et al.*, 2003).

As a first-order test of timing accuracy, we collocated an RS-4D with a Nanometrics Titan accelerometer on an aluminum plate. Both instruments were securely fastened to the plate, and the Titan accelerometer was connected to a Q330 digitizer recording at 100 Hz with a known GPS timing accuracy of ≪ 1 ms (Kromer, 2006). We then subjected the plate to a strong ($> 1g$), impulsive, vertical acceleration and compared with the waveforms of the two sensors to quantify any timing errors in the RS-4D. This test was carried out 10 times over the course of two days.

During these tests, we observed that the strong acceleration signal on the RS-4D always lagged the signal recorded on the Titan by two samples (20 ms). Although the magnitude of this error agrees well with previous studies of seismic equipment using NTP timing (Frassetto *et al.*, 2003), the consistency of the lag is unique. We additionally analyzed earthquake data from small ($M_D < 2.0$), local events around ASL during a time period when the RS-4Ds were collocated in a surface vault with an STS-2 and Trillium Compact as discussed in the Self-Noise section. Figure 5b shows ~1 s of data windowed around the *S*-wave arrival of a local M_D 1.7 event on 25 April 2018. There are several occurrences during the arrival of larger amplitude signals when the RS-4D appears to begin lagging the other instruments by a sample (~10 ms, red circles). We suspect that these lags arise when larger loads on the Raspberry Pi board cause delays in evaluating the timing offsets with an NTP reference server. However, we are unable to isolate the origin of these discrepancies (i.e., determine whether they are produced by the sensor, digitizer, or both). We anticipate that recorded arrival times of seismic phases on Raspberry Shakes may be systematically delayed by up to 20 ms depending on the amplitude of the phase.

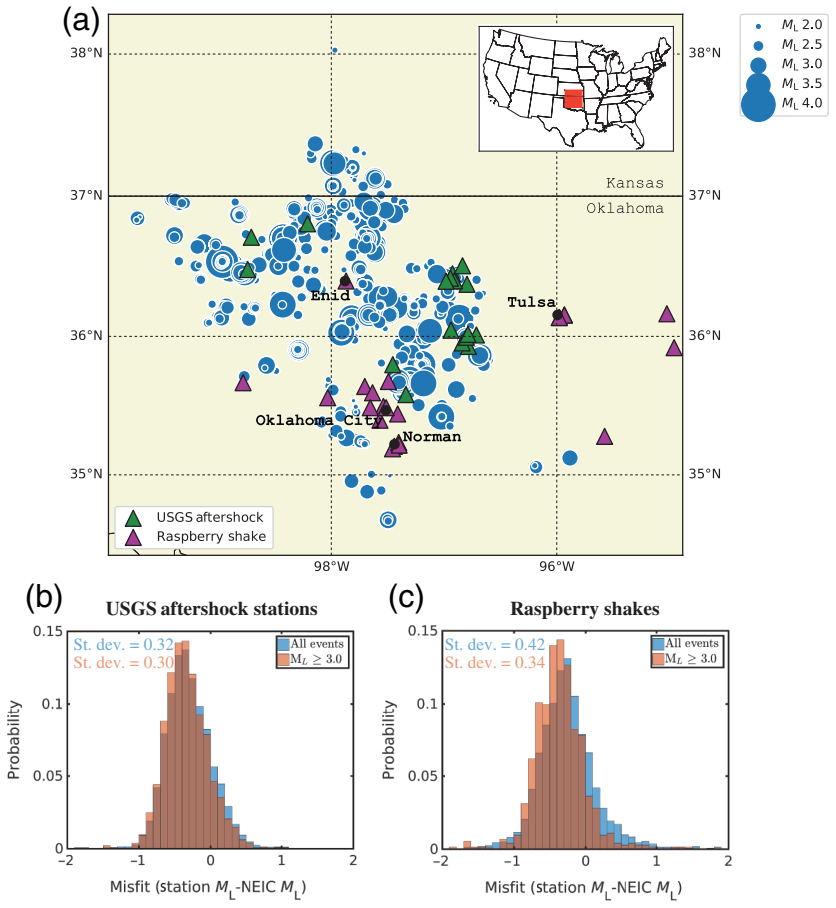

▲ **Figure 6.** (a) USGS aftershock seismic stations (green triangles) and Raspberry Shakes (magenta triangles) that recorded local Oklahoma and Kansas earthquakes (blue circles) between 1 January 2017 and 1 April 2018. Histograms of the misfit between individual, vertical component station local magnitude (M_L) estimates compared with the reported National Earthquake Information Center (NEIC) M_L are shown for both the (b) USGS aftershock deployment stations and (c) Raspberry Shakes as well as the standard deviation (st. dev.) of the misfits.

FIELD APPLICATION: REGIONAL EVENT MAGNITUDE ESTIMATION IN OKLAHOMA

Methods

To evaluate how the Raspberry Shake geophone's relatively high self-noise levels could impact characterization of local events, we compute local earthquake magnitude (M_L) using seismic stations throughout Oklahoma. Oklahoma stations were selected because this region has recently become one of the most seismically active areas in the United States (e.g., Keranen *et al.*, 2014), and several hobbyists in the state have responded by installing personal Raspberry Shake seismographs. Regional earthquakes from all 17 USGS aftershock stations in Oklahoma (network code GS; Albuquerque Seismological Laboratory/U.S. Geological Survey [ASL/USGS], 1980), and 23 privately operated Raspberry Shakes (RS-1Ds and RS-4Ds) between 1 January 2017 and 1 April 2018 were analyzed (Fig. 6a). We use all events within 1.5° of each station with $M_L \geq 2.0$ as reported by the USGS National Earthquake Information Center (NEIC). In total, we processed 6973 event–USGS station pairs and 3548 event–Raspberry Shake pairs.

To estimate M_L for each event–station pair, we begin by selecting a 1-min time window beginning 5 s before the origin time. We then remove the instrument response and convolve the resulting ground motion with the response of a Wood–Anderson seismometer following the methodology of Borman (2013). Additionally, a signal-to-noise ratio (SNR) is calculated by performing an identical procedure for a 1-min time window beginning 2 min before the event origin time. Finally, M_L is calculated as

$$M_L = \log_{10}(x) + 1.11\log_{10}(r) + 0.00189r - 2.09,$$

in which x is the largest displacement in nanometers measured on the vertical component of the event time window and r is the hypocentral distance in kilometers. We note that this calculation is traditionally carried out on the horizontal components, but this is not possible with the Raspberry Shake 1Ds and 4Ds because they only have a vertical-component geophone. We anticipate that this difference will result in M_L estimates that are systematically ~0.3 lower than the NEIC estimates, because local events have been observed to have roughly twice as much ground acceleration as the vertical (e.g., Kalkan and Graizer, 2007). However, when evaluating if noise is influencing this measurement, we are more interested in the standard deviation (st. dev.) of the observations, which is unaffected by this constant. Finally, for each event, we record the difference between the M_L estimated from each GS station or Raspberry Shake and the NEIC's reported M_L (Fig. 6b,c).

RESULTS

For the full-event catalog, including events as small as M_L 2.0, the median misfit (station M_L–NEIC M_L) and 1σ st. dev. is -0.25 ± 0.42 for Raspberry Shakes and -0.30 ± 0.32 for GS stations (Fig. 6b,c). A median misfit > -0.3 and a larger st. dev. for the Raspberry Shake stations indicate that magnitude estimates from Raspberry Shakes tend to be slightly higher and less consistent than estimates from GS stations. However, if events of only $M_L \geq 3.0$ are considered, the median misfit and st. dev. for Raspberry Shake stations (-0.36 ± 0.34) begin to approach the values reported for GS stations (-0.33 ± 0.30). We suspect that these observations can be attributed to the relatively high self-noise levels of the Raspberry Shakes.

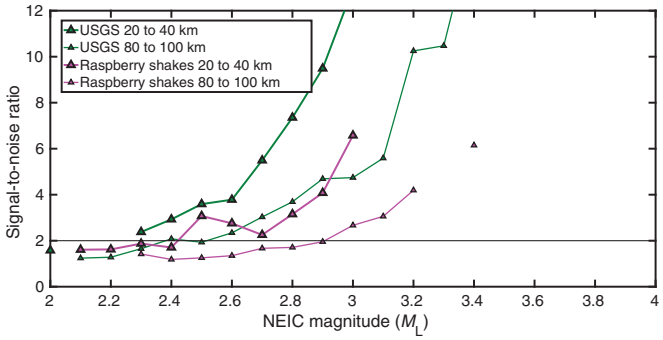

▲ **Figure 7.** Median signal-to-noise ratios (SNRs) for USGS aftershock deployments and Raspberry Shakes as a function of NEIC local magnitude estimates. Station distances of 20–40 km (large triangles) and 80–100 km (smaller triangles) from the event epicenters are plotted. An SNR of 2 (black line) is assumed to be required to record the ground motion with high fidelity.

To test the hypothesis that the high self-noise levels of the Raspberry Shakes could result in overestimation of earthquake magnitudes, we plot median SNRs for both USGS aftershock stations and Raspberry Shakes located at distances of 20–40 km and 80–100 km as a function of NEIC M_L (Fig. 7). To mitigate potential biases arising from limited observations, we require a minimum of 10 SNR estimates at a given distance and NEIC magnitude. We found that for both distance ranges, the USGS aftershock stations always have a higher SNR for a given magnitude event than the Raspberry Shakes. Assuming an SNR of 2 (6 dB) is required to attain an estimate of true ground motion not contaminated by instrument or local site noise, a USGS aftershock station located at 20–40 km from the epicenter of an earthquake would record an event as small as $M_L \sim 2.2$ with high fidelity, but a Raspberry Shake would require at least a M_L 2.5. Similarly, at 80–100 km, a USGS aftershock station can accurately record down to an $M_L \sim 2.5$, but the Raspberry Shakes require a M_L 2.9.

DISCUSSION

Because the Raspberry Shake sensors are typically installed by hobbyists in private residences, the local site amplification effects are likely to be highly variable (e.g., Şafak, 1999). Thus, the observation that Raspberry Shake M_L misfits have a higher st. dev. than USGS aftershock stations could be explained by the highly heterogeneous locations in which these stations are installed. However, this variability in local siting does not readily explain the substantial drop in the st. dev. of misfits when only considering larger ($M_L \geq 3.0$) events. We instead attribute this observation, as well as lower SNRs recorded on the Raspberry Shakes, to the higher self-noise levels of these sensors.

In particular, the idle tones of these instruments fall within the "flat" region of a Wood–Anderson seismometer (e.g., Wang *et al.*, 1989) and will not be attenuated when estimating M_L. Thus, earthquakes that fall below the idle tone noise of the Raspberry Shakes will have the largest signals corresponding to instrumentation noise as opposed to actual ground motion. When automatically picking the largest amplitude signals within a time window around an event, this results in overestimation of the magnitude of these events. Recent updates to the Raspberry Shakes to eliminate the idle tone (RS-1D v.7, RS-3D v.5, RS-4D v.6; Branden Christensen, written comm., 2018) should resolve this issue.

The 0.2- to 5-Hz idle tones found on the early versions of the RS-1D are particularly problematic, because they additionally fall below the corner frequency of local earthquakes (e.g., Shi *et al.*, 1998). For low-SNR events, this idle tone noise will artificially amplify the true ground-motion signal at the idle tone frequency in a manner similar to the secondary microseism observations shown in Figure 2a. This will again result in overestimation of earthquake magnitude for small-amplitude signals. We note that this systematic overestimate of earthquake magnitude only occurs when the SNR is low and that larger events ($M_L > \sim 3.0$ at 100 km) should still be recorded with high fidelity. This explains why both the st. dev. and median estimate of M_L for the Raspberry Shakes become more consistent with GS stations when only considering these larger events (Fig. 6c).

SUMMARY OF INSTRUMENT PERFORMANCE

Overall, we found that the RS-4D performed within the specifications as described by OSOP. The sensitivity of both the geophone and accelerometers was easily within the manufacturer's specification of 10%, and with the exception of a few accelerometer axes, all components were within 5% of nominal. We did observe that the nominal sensitivities of the accelerometers were systematically ~4.3% too low, which would result in slight overestimates of ground acceleration when using the response provided by OSOP. Although these errors in response are four to five times larger than we observed for the instrumentation used in USGS aftershock deployments (Anthony *et al.*, 2017), we anticipate this accuracy will be acceptable for densification of local and regional earthquake monitoring networks. We additionally note that the higher frequency (> 1 Hz) signals that these sensors are targeted at recording may be altered by ≫ 5% by local site amplification (e.g., Phillips and Aki, 1986), and this variability in the instrument sensitivity could be insignificant when analyzing earthquake data.

With a reliable network connection, we observed timing errors no greater than 20 ms. These errors typically manifested as a systematic lag during the arrival of large amplitude seismic phases. These lags could prove problematic when correlating high-frequency waveforms between individual shakes or measuring changes in arrival times of phases across a very dense network. However, *P*-wave travel-time residuals for regional events recorded on relatively dense networks often exceed 0.5 s even when using a regional velocity model (e.g., Darold *et al.*, 2015). We thus expect unmodeled variations in velocity caused by local geologic structure will play a much larger role in timing errors when locating events than the ≤ 0.02 s lag introduced by NTP timing.

The largest drawbacks to the RS-4D are the relatively high self-noise levels of the instruments. The geophones have similar self-noise levels as the Kinemetrics EpiSensors used in USGS

aftershock and ANSS deployments and therefore are expected to have similar abilities to characterize earthquakes as these sensors. The MEMS accelerometers have such high noise levels that they will likely only record local (~10 km) events of $M > 2.5$ and regional (~100 km) events of $M > 5.0$. The main benefits of upgrading from the RS-1D to the RS-4D are the ability to record strong ground motion on the horizontal components and attain on-scale recordings of large ($M > \sim 6$), local events.

In general, ambient seismic background noise will not be accurately recorded by the Raspberry Shake geophones, with the exception of extremely noisy environments (e.g., volcanoes, near-coastal installations). Over the three months that we had an RS-4D installed in the surface vault, we found that we were only able to identify the surface waves on the geophone of teleseismic earthquakes of $\sim M$ 6.5 or greater. Thus, Raspberry Shakes are not suitable for studies using ambient seismic noise or teleseismic events.

Instead, the RS-4D and its derivatives are much better suited for the characterization of local and regional events. To assess the potential of Raspberry Shake sensors to be integrated into regional networks, we compared individual station estimates of local earthquake magnitudes in Oklahoma using both USGS aftershock deployments and privately operated Raspberry Shakes within the state. We found the higher self-noise levels of the Raspberry Shakes, in particular the idle tones found on earlier versions, likely contributed to slight overestimates of local earthquake magnitudes for small ($M_L < 3$ events). For events larger than M_L 3, the variability in magnitude estimates for the Raspberry Shakes is very similar to USGS aftershock deployments. We conclude that the low cost of such sensors combined with their ease of installation and transmission of near-real-time data should make them an ideal candidate for use in densification of seismic networks designed to identify and characterize local and regional events. However, it is important for network operators to understand the relative performance and drawbacks of these stations compared with broadband sensors.

DATA AND RESOURCES

All laboratory data were collected at the U.S. Geological Survey (USGS) Albuquerque Seismological Laboratory (ASL/USGS, 1980) and are available through the Incorporated Research Institutions for Seismology (IRIS) Data Management Center under network code GS. All Raspberry Shake data from Oklahoma are freely available and were downloaded from https://fdsnws.raspberryshakedata.com (last accessed April 2018). Additionally, the IRIS nominal response library is available at http://www.iris.edu/NRL (last accessed March 2018). All MATLAB (www.mathworks.com/products/matlab, last accessed May 2018) and ObsPy (Beyreuther *et al.*, 2010) codes used in this analysis is freely available on GitHub (https://github.com/reanthony-usgs/Raspberry_Shakes, last accessed October 2018). Raspberry Shake technical specifications may be found at https://manual.raspberryshake.org/specifications.html#techspecs (last accessed August 2018). Network transfer protocol is available at www.ntp.org (last accessed March 2018).

ACKNOWLEDGMENTS

The authors would like to thank Branden Christensen and Angel Rodriguez at OSOP for discussing a number of questions that came up while testing these instruments. The authors also thank them for providing us additional units for testing with the changed idle tone frequency. Timothy Lindgren set up the Raspberry Shake 4Ds (RS-4Ds) on the local Albuquerque Seismological Laboratory (ASL) network and Vernon Stoup customized the flip box used to measure the accelerometer sensitivities. Tyler Storm assisted in producing the metadata and sent all data and metadata created at ASL for this article to the Incorporated Research Institutions for Seismology Data Management Center (IRIS-DMC). The authors thank Will Yeck for help with identifying the correction equation used to estimate the local earthquake magnitudes and Bob Hutt for helping to test an earlier version of the sensor. The presentation of this article benefitted greatly from reviews by David Oppenheimer, Mairi Litherland, Zhigang Peng, Janet Slate, and two anonymous reviewers. This research was supported by the Mendenhall Postdoctoral Fellowship program of the U.S. Geological Survey (USGS).

Any use of trade, product, firm, or product names is for descriptive purposes only and does not imply endorsement by the U.S. Government.

REFERENCES

Advanced National Seismic System (ANSS) Working Group (2008). Instrumentation guidelines for the Advanced National Seismic System [Working group on instrumentation, siting, installation, and site metadata of the Advanced National Seismic System technical integration committee], *U.S. Geol. Surv. Open-File Rept. 2008-1262*, 41 pp.; available at http://pubs.usgs.gov/of/2008/1262/pdf/OF08-1262_508.pdf (last accessed July 2018)

Ahern, T., R. Casey, D. Barnes, R. Benson, T. Knight, and C. Trabant (2009). *SEED Reference Manual, Version 2.4*, available at http://www.fdsn.org/seed_manual/SEEDManual_V2.4.pdf (last accessed February 2018).

Aki, K., and P. G. Richards (2002). *Quantitative Seismology*, Second Ed., University Science Books, Sausalito, California, 700 pp.

Albuquerque Seismological Laboratory/U.S. Geological Survey (ASL/USGS) (1980). U.S. Geological Survey Networks, *International Federation of Digital Seismograph Networks, Other/Seismic Network*, doi: 10.7914/SN/GS.

Anthony, R. E., R. C. Aster, D. Wiens, A. Nyblade, S. Anandakrishnan, A. Huerta, J. P. Winberry, T. Wilson, and C. Rowe (2015). The seismic noise environment of Antarctica, *Seismol. Res. Lett.* **86,** 89–100.

Anthony, R. E., A. T. Ringler, and D. C. Wilson (2017). Improvements in absolute seismometer sensitivity calibration using local earth gravity measurements, *Bull. Seismol. Soc. Am.* **108,** 503–510.

Ben-Zion, Y., F. L. Vernon, Y. Ozakin, D. Zigone, Z. E. Ross, H. Meng, M. White, J. Reyes, D. Hollis, and M. Barklage (2015). Basic data features and results from a spatially dense seismic array on the San Jacinto fault zone, *Geophys. J. Int.* **202,** 370–380.

Beyreuther, M., R. Barsch, L. Krischer, T. Megies, Y. Behr, and J. Wassermann (2010). ObsPy: A python toolbox for seismology, *Seismol. Res. Lett.* **81,** 530–533.

Borman, P. (2013). Working group on magnitude measurements, *Summary of Magnitude Working Group Recommendations on Standard Procedures for Determining Earthquake magnitudes from Digital Data*, Updated Version 27 March 2013, available at ftp://ftp.iaspei.org/pub/

commissions/CSOI/Summary_WG_recommendations_20130327.pdf (last accessed April 2018).
Clinton, J. F., and T. H. Heaton (2002). Potential advantages of a strong-motion velocity meter over a strong-motion accelerometer, *Seismol. Res. Lett.* **73,** 332–342.
Darold, A. P., A. A. Holland, J. K. Morris, and A. R. Gibson (2015). Oklahoma earthquake summary report 2014, *Oklahoma Geol. Surv. Open-File Rept.*, 1–46.
Doody, C. D., A. T. Ringler, R. E. Anthony, D. C. Wilson, A. A. Holland, C. R. Hutt, and L. D. Sandoval (2017). Effects of thermal variability on broadband seismometers: Controlled experiments, observations, and implications, *Bull. Seismol. Soc. Am.* **108,** 493–502.
Evans, J. R., R. M. Allen, A. I. Chung, E. S. Cochran, R. Guy, M. Hellweg, and J. F. Lawrence (2014). Performance of several low-cost accelerometers, *Seismol. Res. Lett.* **85,** 147–158.
Frassetto, A., T. J. Owens, and P. Crotwell (2003). Evaluating the Network Time Protocol (NTP) for timing in the South Carolina earth physics project (SCEPP), *Seismol. Res. Lett.* **74,** 649–652.
Hansen, S. M., and B. Schmandt (2015). Automated detection and location of microseismicity at Mount St. Helens with a Large-N geophone array, *J. Geophys. Res.* **52,** 7390–7397.
Hutt, C. R., A. T. Ringler, and L. S. Gee (2017). Broadband seismic noise attenuation versus depth at the Albuquerque seismological laboratory, *Bull. Seismol. Soc. Am.* **107,** 1402–1412.
Incorporated Research Institutions for Seismology Data Management Center (IRIS-DMC) (2014). *Data Services Products: Noise Toolkit PDF-PSD Bundle*, doi: 10.17611/DP/NTK.2.
Kalkan, E., and V. Graizer (2007). Multi-component ground motion response spectra for coupled horizontal, vertical, angular accelerations, and tilt, *ISET J. Earthq. Technol.* **44,** 259–284.
Keranen, K. M., M. Weingarten, G. A. Abers, B. A. Bekins, and S. Ge (2014). Sharp increase in central Oklahoma seismicity since 2008 induced by massive wastewater injection, *Science* **345,** 448–451.
Krischer, L., T. Megies, R. Barsch, M. Beyreuther, T. Lecocq, C. Caudin, and J. Wassermann (2015). ObsPy: A bridge for seismology into the scientific Python ecosystem, *Comput. Sci. Discov.* **8,** 014003, doi: 10.1088/1749-4699/8/1/014003.
Kromer, R. P. (2006). *Evaluation of the Kinemetrics/Quanterra Q330HR Remote Seismic System for IRIS/GSN*, Sandia National Laboratories, 103 pp.
Kuyuk, H. S., and R. M. Allen (2013). Optimal seismic network density for earthquake early warning: A case study from California, *Seismol. Res. Lett.* **84,** 946–954.
Lin, F., D. Li, R. W. Clayton, and D. Hollis (2013). High-resolution 3D shallow crustal structure in Long Beach, California, Application of ambient noise tomography on a dense seismic array, *Geophysics* **78,** Q45–Q56.
Nelder, J. A., and R. Mead (1965). A simplex method for function minimization, *Comput. J.* **7,** 308–313.
Pavlis, G. L., and F. L. Vernon (1994). Calibration of seismometers using ground noise, *Bull. Seismol. Soc. Am.* **84,** 1243–1255.
Peterson, J. (1993). Observation and modeling of seismic background noise, *U.S. Geol. Surv. Open-File Rept. 93-322*, 94 pp.
Phillips, W. S., and K. Aki (1986). Site amplification of coda waves from local earthquakes in central California, *Bull. Seismol. Soc. Am.* **76,** 627–648.
Reiss, J. D. (2008). Understanding sigma-delta modulation: The solved and unsolved issues, *J. Audio Eng. Soc.* **56,** 49–64.
Riahi, N., and P. Gerstoft (2015). The seismic traffic footprint: Tracking trains, aircraft, and cars seismically, *Geophys. Res. Lett.* **42,** 2674–2681.
Ringler, A. T., and C. R. Hutt (2010). Self-noise models of seismic instruments, *Seismol. Res. Lett.* **81,** 972–983.
Ringler, A. T., R. E. Anthony, M. S. Karplus, A. A. Holand, and D. C. Wilson (2018). Laboratory test of three Z-land fairfield nodal 5-Hz, three-component sensors, *Seismol. Res. Lett.* **89,** doi: 10.1785/0220170236.
Ringler, A. T., J. R. Evans, and C. R. Hutt (2015). Self-noise models of five commercial strong-motion accelerometers, *Seismol. Res. Lett.* **86,** 1143–1147.
Ringler, A. T., A. A. Holland, and D. C. Wilson (2017). Repeatability testing of a small broadband sensor in the Albuquerque Seismological Laboratory underground vault, *Bull. Seismol. Soc. Am.* **107,** 1557–1563.
Romeo, G. (2012). Whale watching: effects of strong signals on Lippmann style seismometers, *J. Seismol.* **16,** 25–34.
Şafak, E. (1999). Wave-propagation formulation of seismic response of multistory buildings, *J. Struct. Eng.* **125,** 426–437.
Schmandt, B., and R. W. Clayton (2013). Analysis of teleseismic *P* waves with a 5200-station array in Long Beach, California: Evidence for an abrupt boundary to Inner Borderland rifting, *J. Geophys. Res.* **118,** 5320–5338.
Schmandt, B., D. Gaeuman, R. Stewart, S. M. Hansen, V. C. Tsai, and J. Smith (2017). Seismic array constraints on reach-scale bedload transport, *Geology* 299–302, doi: 10.1130/G38639.1.
Shi, J., W. Kim, and P. G. Richards (1998). The corner frequencies and stress drops of intraplate earthquakes in the northeastern United States, *Bull. Seismol. Soc. Am.* **88,** 531–542.
Sleeman, R., A. van Wettum, and J. Trampert (2006). Three-channel correlation analysis: A new technique to measure instrumental noise of digitizers and seismic sensors, *Bull. Seismol. Soc. Am.* **96,** 258–271.
Steim, J. M. (1986). The very-broad-band seismograph, *Ph.D. Dissertation*, Department of Geological Sciences, Harvard University, Cambridge, Massachusetts.
Sweet, J. R., K. R. Anderson, S. Bilek, M. Brudzinski, X. Chen, H. DeShon, C. Hayward, M. Karplus, K. Keranen, C. Langston, *et al.* (2018). A community experiment to record the full seismic wavefield in Oklahoma, *Seismol. Res. Lett.* doi: 10.1785/0220180079.
Templeton, M. (2017). IRIS library of nominal response for seismic instruments, *Incorporated Research Institutions for Seismology*, doi: 10.17611/S7159Q.
Wang, J.-H., C.-C. Liu, and Y.-B. Tsai (1989). Local magnitude determined from a simulated Wood–Anderson seismograph, *Tectonophysics* **166,** 15–26.
Wielandt, E., and M. Zumberge (2013). Measuring seismometer nonlinearity on a shake table, *Bull. Seismol. Soc. Am.* **103,** 2247–2256.
Wolin, E., S. van der Lee, T. A. Bollmann, D. A. Wiens, J. Revenaugh, F. A. Darbyshire, A. W. Frederiksen, S. Stein, and M. E. Wysession (2015). Seasonal and diurnal variations in long-period noise at SPREE stations: The influence of soil characteristics on shallow stations' performance, *Bull. Seismol. Soc. Am.* **105,** 2433–2452.

Robert E. Anthony
Adam T. Ringler
David C. Wilson
U.S. Geological Survey
Albuquerque Seismological Laboratory
P.O. Box 82010
Albuquerque, New Mexico 87198-2010 U.S.A.
reanthony@usgs.gov
aringler@usgs.gov
dwilson@usgs.gov

Emily Wolin
U.S. Geological Survey
Earthquake Science Center
1711 Illinois Street
Golden, Colorado 80401 U.S.A.
ewolin@usgs.gov

Published Online 14 November 2018